

Quadratic quasi-normal mode dependence on linear mode parity

Patrick Bourg,¹ Rodrigo Panosso Macedo,² Andrew Spiers,^{3,4} Benjamin Leather,⁵ Béatrice Bonga,¹ and Adam Pound⁶

¹*Institute for Mathematics, Astrophysics and Particle Physics,*

Radboud University, Heyendaalseweg 135, 6525 AJ Nijmegen, The Netherlands

²*Niels Bohr International Academy, Niels Bohr Institute, Blegdamsvej 17, 2100 Copenhagen, Denmark*

³*School of Mathematical Sciences & School of Physics and Astronomy,
University of Nottingham, University Park, Nottingham, NG7 2RD, UK*

⁴*Nottingham Centre of Gravity, University of Nottingham, University Park, Nottingham, NG7 2RD, UK*

⁵*Max Planck Institute for Gravitational Physics (Albert Einstein Institute), Am Mühlenberg 1, Potsdam 14476, Germany*

⁶*School of Mathematical Sciences and STAG Research Centre,
University of Southampton, Southampton, SO17 1BJ, United Kingdom*

(Dated: May 20, 2024)

Quasi-normal modes (QNMs) uniquely describe the gravitational-wave ringdown of post-merger black holes. While the linear QNM regime has been extensively studied, recent work has highlighted the importance of second-perturbative-order, quadratic QNMs (QQNMs) arising from the nonlinear coupling of linear QNMs. Previous attempts to quantify the magnitude of these QQNMs have shown discrepant results. Using a new hyperboloidal framework, we resolve the discrepancy by showing that the QQNM/QNM ratio is a function not only of the black hole parameters but also of the ratio between even- and odd-parity linear QNMs: the ratio QQNM/QNM depends on what created the ringing black hole, but *only* through this ratio of even- to odd-parity linear perturbations.

Introduction.—After the merger of two black holes (BHs), the distorted remnant BH rings down towards a stationary state through its emission of gravitational waves (GWs). The signal associated with this process is well modelled by a superposition of exponentially damped sinusoids, with complex frequencies given by the so-called quasi-normal modes (QNMs) [1–4]. For an isolated system within General Relativity (GR), these QNM frequencies are uniquely determined by the mass and spin of the final BH. Each frequency $\omega_{\ell m}$ is characterised by three integers: polar and azimuthal indices (ℓ, m) associated with a projection onto spherical harmonics on the celestial sphere, and an overtone index $n = 0, 1, \dots$ that enumerates the frequencies for a given angular mode.

Inspired by the uniqueness of the QNM spectrum, the BH spectroscopy program [5–7] aims at extracting multiple QNMs from ringdown signals in order to perform stringent tests of GR, probe the BH geometry, and constrain features of the surrounding environment [1–3]. Measurements of the dominant QNM, $(\ell, m, n) = (2, \pm 2, 0)$, in GW signals are well established [8–10]. The detection of higher overtones and higher angular modes is still under debate [11–24], but future GW detectors such as the Einstein Telescope and LISA are expected to observe these higher modes regularly. Current forecasts predict 20–50 events per year with at least two detectable QNMs for stellar-mass binaries [25, 26] and even $\sim 5 - 8$ QNMs for massive BH binaries with LISA [7, 27].

Historically, the BH spectroscopy program has been entirely based on linear BH perturbation theory (BHPT) [1–6], and forecasts for future QNM detections assume only linear QNM frequencies. However, GR is a nonlinear theory, and recent milestone results have shown that BH spectroscopy must also account for second-order, quadratic perturbations, which can dominate over linear overtones [20, 28–34]. In these quadratic perturbations, a

new set of characteristic frequencies arises: the so-called quadratic QNMs (QQNMs) $\omega_{\ell_1 m_1 n_1 \times \ell_2 m_2 n_2} = \omega_{\ell_1 m_1 n_1} + \omega_{\ell_2 m_2 n_2}$, which result from the coupling of two linear QNMs. A recent analysis indicates that the Einstein Telescope and Cosmic Explorer could detect QQNMs in up to a few tens of events per year [35]. While the predictions for LISA depend sensitively on the astrophysical massive BH formation models, the most optimistic scenario allows for up to $\mathcal{O}(1000)$ events with detectable QQNMs in LISA’s nominal 4-year observation time [35].

Spurred by these developments, there has been a spate of recent work devoted to analysing QQNMs and their impact on BH spectroscopy. Most calculations have been based on extracting modes from fully nonlinear numerical relativity (NR) simulations of BH binary evolutions, but a number of recent calculations have also been performed using second-order BHPT [34, 36, 37]. These calculations have generally focused on a single measure of the significance of QQNMs: the ratio between a given QQNM mode amplitude and the amplitude(s) of the linear parent mode(s) that generate it. Perhaps surprisingly, different analyses have led to conflicting values of the ratio, even in the simplest case of non-rotating BHs.

It has been suggested that the discrepancies in Schwarzschild could be due to the freedom to excite both even- and odd-parity perturbations [34]. We find that this can explain the discrepancy in previous QQNM analyses, but this property is not restricted to a Schwarzschild background; it also holds in Kerr. Consequently, we observe that reported QQNM/QNM ratios in the literature often lack sufficient information to describe the relationship between linear and non-linear QNMs fully. To shift this paradigm, we establish that the ratio depends not only on the BH parameters, but also on the properties of the system that created the ringing BH. Specifically, it is a function of the ratio between the

amplitudes of even- and odd-parity linear QNMs; this ratio will depend on the degree to which the progenitor system possessed equatorial (up-down) symmetry.

As a proof of principle, we make this argument precise, and present numerical results for the QQNM/QNM ratio, in the simple case of Schwarzschild spacetime. We discuss the generalisation to the most generic case in the conclusion. Our calculation utilizes a novel code combining two critical components: a hyperboloidal frequency-domain framework that allows us to directly and accurately compute the physical waveform without requiring regularization [38–45]; and a covariant second-order BHPT formalism [46, 47]. By controlling the geometrical aspects of the problem and using the mode-coupling tools of Ref. [46], we are able to fine-tune the first-order dynamics to single out any number of linear modes and obtain the quadratic contribution from the linear even- and odd-parity sectors semi-analytically.

Black hole perturbation theory.—In BHPT we expand the spacetime metric in the form $g_{ab} + \varepsilon h_{ab}^{(1)} + \varepsilon^2 h_{ab}^{(2)} + \dots$, where g_{ab} is a Kerr metric and $\varepsilon = 1$ counts perturbative orders. In vacuum, the perturbations satisfy the Einstein equations

$$\varepsilon \delta G_{ab}[h_{cd}^{(1)}] + \varepsilon^2 (\delta G_{ab}[h_{cd}^{(2)}] + \delta^2 G_{ab}[h_{cd}^{(1)}]) + \dots = 0, \quad (1)$$

where δG_{ab} is the linearized Einstein tensor and $\delta^2 G_{ab}[h_{cd}^{(1)}]$ is quadratic in $h_{cd}^{(1)}$ [48].

At linear order all nontrivial information in $h_{ab}^{(1)}$ is encoded in the linearized Weyl scalar $\Psi_4^{(1)}$, which satisfies the vacuum Teukolsky equation $\mathcal{O}[\Psi_4^{(1)}] = 0$, where \mathcal{O} is a linear second-order differential operator [49, 50].

We adopt compactified hyperboloidal coordinates $(\tau, \sigma, \theta, \varphi)$ [39, 42], in which constant- τ slices connect the future horizon \mathcal{H}^+ (at compactified radial coordinate $\sigma = 1$) to future null infinity \mathcal{J}^+ (at $\sigma = 0$). Using the hyperboloidal time τ , we introduce the frequency-domain field $\psi_4^{(1)}$ via a Laplace (or Fourier) transform,

$$\psi_4^{(1)}(\sigma, \theta, \varphi; s) = \int_0^\infty \Psi_4^{(1)}(\tau, \sigma, \theta, \varphi) e^{-s\tau} d\tau. \quad (2)$$

The complex Laplace parameter s is related to the usual complex frequency ω by $s = -i\omega$. We next separate the Teukolsky equation into an angular and radial part by decomposing $\psi_4^{(1)}$ into spin-weighted spheroidal harmonics [49–51],

$$\psi_4^{(1)} = \mathcal{Z}(\sigma) \sum_{\ell m} \tilde{\psi}_{\ell m}^{(1)}(\sigma; s) {}_{-2}S_{\ell m}(\theta, \varphi; s). \quad (3)$$

Here $\mathcal{Z}(\sigma)$ serves to factor out the dominant behavior near \mathcal{H}^+ and \mathcal{J}^+ ; a linear vacuum perturbation $\Psi_4^{(1)}$ scales quadratically with distance from the horizon near \mathcal{H}^+ and decays inversely with distance toward \mathcal{J}^+ [42, 48], motivating us to choose $\mathcal{Z}(\sigma) \propto \sigma(1 - \sigma)^2$. Because we use hyperboloidal slices [42, 44, 52], the modes $\tilde{\psi}_{\ell m}^{(1)}$ are

smooth on the entire domain, $\sigma \in [0, 1]$, and because we factor out \mathcal{Z} we can directly compute the waveform from $\tilde{\psi}_{\ell m}^{(1)}$ at $\sigma = 0$.

The Laplace transform and spheroidal-harmonic expansion leaves us with a radial Teukolsky equation, $\mathcal{D}_{\ell m}[\tilde{\psi}_{\ell m}^{(1)}(\sigma; s)] = 0$, where $\mathcal{D}_{\ell m}$ is a linear second-order radial operator. In the hyperboloidal setup, linear QNMs are the solutions to this equation that satisfy regularity conditions at both ends ($\sigma = 0$ and 1). Such solutions only exist for the countable set of QNM frequencies $s_{\ell m n}$, and we denote them $\tilde{\psi}_{\ell m n}^{(1)}(\sigma) := \tilde{\psi}_{\ell m}^{(1)}(\sigma; s_{\ell m n})$.

Given a set of QNM solutions, $\tilde{\psi}_{\ell m n}^{(1)}$, the inverse Laplace transform yields a time-domain solution of the form [39]

$$\Psi_4^{(1)} = \mathcal{Z}(\sigma) \sum_{\ell m n} A_{\ell m n} \tilde{\psi}_{\ell m n}^{(1)}(\sigma) e^{s_{\ell m n} \tau} {}_{-2}S_{\ell m}(\theta, \varphi; s_{\ell m n}). \quad (4)$$

Since QNM solutions are only defined up to an overall constant factor, the $A_{\ell m n}$ are arbitrary (complex) excitation coefficients, and we set $\tilde{\psi}_{\ell m n}^{(1)} = 1$ at \mathcal{J}^+ . In Eq. (4), we neglect late-time tail contributions that generically arise [53]; this choice fixes a pure QNM dynamics at linear order.

Mirror modes and parity.—The azimuthal symmetry of Kerr spacetime causes a symmetry between the $+m$ and $-m$ QNM frequencies [51, 54]

$$s_{\ell -m n} = s_{\ell m n}^*. \quad (5)$$

Additionally, our choice of normalization implies that the corresponding eigenfunctions are related by $\tilde{\psi}_{\ell -m n} = \tilde{\psi}_{\ell m n}^*$. The QNMs with $m \geq 0$ and $m < 0$ are known as the *regular* and *mirror* QNMs, respectively. They decay at the same rate but oscillate in opposite directions.

In Schwarzschild spacetime, the frequencies degenerate: prograde and retrograde modes become indistinguishable and m -independent. Nonetheless, QNM frequencies come in complex conjugate pairs, and the full solution can still be written in the form of (4), where one can impose (without loss of generality) the mirror relation in (5).

Most QNM analyses have exclusively considered the regular QNMs. In [54], the importance of including mirror QNMs was demonstrated in linear QNM analyses to reduce systematic uncertainties. In this work, we find that mirror modes also play a crucial role in QQNM analysis.

The ratio between regular and mirror modes, $A_{\ell -m n}/A_{\ell m n}$, is directly related to the ratio between even- and odd-parity contributions to the GW. At \mathcal{J}^+ , the GW (or more strictly, the shear [55]) can be naturally decomposed into even-parity (Y_{AB}) and odd-parity (X_{AB}) tensor harmonics [46, 56],

$$h_{AB}^{(1)} = r^2 \mathcal{Z}(\sigma) \sum_{\ell m n} (C_{\ell m n}^+ Y_{AB}^{\ell m} + C_{\ell m n}^- X_{AB}^{\ell m}) e^{s_{\ell m n} \tau}, \quad (6)$$

where it is understood that this applies in the $r \rightarrow \infty$ ($\sigma \rightarrow 0$) limit, $\theta^A = (\theta, \varphi)$, the factor of r^2 corresponds to the natural scaling of angular components, $C_{\pm}^{\ell m n}$ are

constant (complex) amplitudes, and $\tau = u$ (the usual outgoing null coordinate).

For comparison, $\Psi_4^{(1)}$ at \mathcal{J}^+ can be decomposed into the closely-related spin-weight -2 spherical harmonics ${}_{-2}Y_{\ell m}$ (requiring a projection from spheroidal harmonics, except in the Schwarzschild case where ${}_{-2}S_{\ell m}$ reduces to ${}_{-2}Y_{\ell m}$). To relate the amplitudes $A_{\ell mn}$ to $C_{\ell m}^{\pm}$, we use the relations between harmonics in Ref. [46] together with the fact that $\lim_{r \rightarrow \infty} \Psi_4^{(1)} = -\frac{1}{2} \lim_{r \rightarrow \infty} \ddot{h}_{\bar{m}\bar{m}}$, where $\bar{m}^A = \frac{1}{\sqrt{2r}}(1, i \csc \theta)$. A short calculation reveals

$$A_{\ell mn} = -\frac{s_{\ell mn}^2}{4} \lambda_{\ell,2} (C_{\ell mn}^+ - iC_{\ell mn}^-), \quad (7)$$

$$A_{\ell -mn}^* = -(-1)^m \frac{s_{\ell mn}^2}{4} \lambda_{\ell,2} (C_{\ell mn}^+ + iC_{\ell mn}^-), \quad (8)$$

where $\lambda_{\ell,2} = \sqrt{(\ell+2)!/(\ell-2)!}$. Equation (8) follows from the mirror relation (5) and the fact that the 4D metric perturbation is real, i.e., $C_{\ell -mn}^{\pm} = (-1)^m (C_{\ell mn}^{\pm})^*$.

Equations (7) and (8) imply that the complex ratio $A_{\ell -mn}/A_{\ell mn}$ is a simple function of $C_{\ell mn}^-/C_{\ell mn}^+$. We emphasize that while it is impossible to omit $m < 0$ modes from $h_{AB}^{(1)}$ (as they are required for $h_{AB}^{(1)}$ to be real-valued), it is possible to omit $m < 0$ modes in $\Psi_4^{(1)}$; this corresponds to the particular ratio $C_{\ell mn}^+ = -iC_{\ell mn}^-$.

Quadratic QNMs.—Like at first order, the second-order contribution to the GW is fully encoded in a linear Weyl scalar $\Psi_{4L}^{(2)}$ constructed from $h_{ab}^{(2)}$ [47, 57]. $\Psi_{4L}^{(2)}$ satisfies a “reduced” second-order Teukolsky equation derived from the second-order terms in the Einstein equation (1) [47, 58]:

$$\mathcal{O}[\Psi_{4L}^{(2)}] = -\mathcal{S}[\delta^2 G_{ab}[h_{cd}^{(1)}]] := \tilde{\mathcal{S}}, \quad (9)$$

where \mathcal{S} is a linear second-order differential operator [48].

The source in Eq. (9) depends quadratically on the first-order metric perturbation; schematically,

$$\tilde{\mathcal{S}} \sim \nabla \nabla (\nabla h_{ab}^{(1)})^2. \quad (10)$$

In Schwarzschild [46], the ℓm modes of $\tilde{\mathcal{S}}$ are readily computed from an arbitrary set of first-order ℓm modes using the *Mathematica* package *PerturbationEquations* [59].

We obtain the ℓm modes of $h_{ab}^{(1)}$ using a standard metric reconstruction procedure [48] in the outgoing radiation gauge (ORG), in which $h_{ab}^{(1)}$ is computed from a Hertz potential Φ^{ORG} satisfying the inversion relation

$$\Psi_4^{(1)} = \frac{1}{4} \mathcal{P}'^4 \bar{\Phi}^{\text{ORG}}, \quad (11)$$

where \mathcal{P}' is a derivative along ingoing principal null rays [48]. In terms of this Hertz potential,

$$h_{ab}^{(1)} = 2\text{Re}(\mathcal{S}^\dagger \Phi^{\text{ORG}})_{ab}, \quad (12)$$

where \mathcal{S}^\dagger denotes the adjoint of \mathcal{S} .

Note that $h_{ab}^{(1)}$ depends on both Φ^{ORG} and $\bar{\Phi}^{\text{ORG}}$ and therefore on both Ψ_4 and $\bar{\Psi}_4$ via Eq. (11). Consequently, each QQNM amplitude depends on regular and mirror linear QNM amplitudes. To elucidate this, we consider $\Psi_4^{(1)}$ being composed of a single regular and mirror mode in Schwarzschild spacetime,

$$\Psi_4^{(1)} = \mathcal{Z}(\sigma) \left\{ A_{\ell mn} \tilde{\psi}_{\ell mn}^{(1)}(\sigma) e^{s_{\ell mn} \tau} {}_{-2}Y_{\ell m}(\theta, \phi) + A_{\ell -mn} (\tilde{\psi}_{\ell mn}^{(1)}(\sigma))^* e^{s_{\ell mn}^* \tau} {}_{-2}Y_{\ell -m}(\theta, \phi) \right\}. \quad (13)$$

Equations (10)–(12) show that the second-order source $\tilde{\mathcal{S}}$ depends quadratically on $\Psi_4^{(1)}$ and $\bar{\Psi}_4^{(1)}$. Via our ansatz (13) and Eq. (5), $\tilde{\mathcal{S}}$ is hence composed of three distinct terms,

$$\tilde{\mathcal{S}} = \mathcal{Z}(\sigma) \left\{ \tilde{\mathcal{S}}^{LM}(\sigma) e^{2s_{\ell mn} \tau} {}_{-2}Y_{LM}(\theta, \phi) + \tilde{\mathcal{S}}^{L0}(\sigma) e^{2\text{Re}(s_{\ell mn}) \tau} {}_{-2}Y_{L0}(\theta, \phi) + \tilde{\mathcal{S}}^{L-M}(\sigma) e^{2s_{\ell mn}^* \tau} {}_{-2}Y_{L-M}(\theta, \phi) \right\}, \quad (14)$$

where $L = 2\ell$, and $M = 2m$.

Given the source (14), we solve Eq. (9) following the same procedure as at first order, performing a Laplace transform in hyperboloidal time, decomposing into ℓm modes, and solving the resulting radial equations. The time-domain solution is obtained by applying an inverse Laplace transform, which contains the same modes as the source (14) (in addition to tails and other contributions that we neglect). In particular, it is composed of (L, M) , $(L, 0)$, $(L, -M)$ spherical modes, with associated frequencies $2s_{\ell mn}$, $2\text{Re}(s_{\ell mn})$ and $2s_{\ell mn}^*$. Each of these QQNMs depends on the first-order excitation coefficients in the following way:

$$\left(\Psi_{4L}^{(2)} \right)^{LM} = a^{LM}(\sigma) A_{\ell mn}^2 + b^{LM}(\sigma) A_{\ell mn} A_{\ell -mn}^*, \quad (15)$$

$$\left(\Psi_{4L}^{(2)} \right)^{L0} = a^{L0}(\sigma) A_{\ell mn} A_{\ell -mn} + b^{L0}(\sigma) A_{\ell mn} A_{\ell mn}^* + (b^{L0}(\sigma))^* A_{\ell -mn} A_{\ell -mn}^*, \quad (16)$$

$$\left(\Psi_{4L}^{(2)} \right)^{L-M} = (a^{LM}(\sigma))^* A_{\ell -mn}^2 + (b^{LM}(\sigma))^* A_{\ell mn}^* A_{\ell -mn}. \quad (17)$$

We provide the coefficients (a^{LM} etc.), evaluated at \mathcal{J}^+ , in the Supplemental Material.

Note that one can uniquely determine the two excitation amplitudes of the first-order data, $A_{\ell mn}$ and $A_{\ell -mn}$, up to an overall sign, from the excitations at second order, by solving the system (15)–(17) for $A_{\ell mn}$ and $A_{\ell -mn}$ at a radial point $\sigma = \sigma_0$, for example at \mathcal{J}^+ , $\sigma_0 = 0$. Given the relations (7)–(8), this means that from the QQNMs one can uniquely determine, up to an overall sign (which corresponds to a phase difference of $+\pi$), the contribution of the even and odd sectors of the first-order QNMs. The residual sign ambiguity is due to the fact that the second-order source, and therefore the QQNMs, are invariant under a sign change $\Psi_4^{(1)} \rightarrow -\Psi_4^{(1)}$; see again Eq. (10).

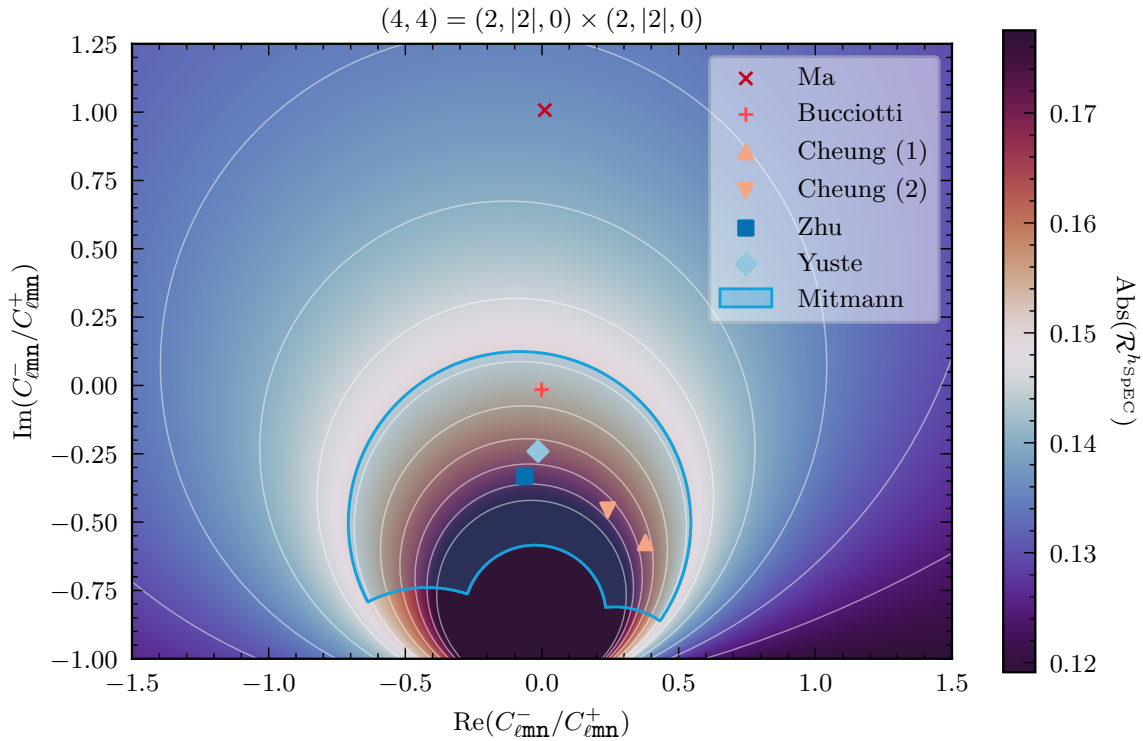


FIG. 1: Contour plot of the ratio $(\mathcal{R}^{h_{\text{SpEC}}})_{(\ell m n) \times (\ell m n)}^{LM}$ as a function of the odd-to-even complex amplitude ratio $C_{\ell m n}^-/C_{\ell m n}^+$ for the quadratic mode $(4, 4) = (2, |2|, 0) \times (2, |2|, 0)$. The solid lines are values of constant amplitude of the QQNM ratio. We have also indicated previous results in the literature: Ma *et al.* (dark red cross) [34]; Bucciotti *et al.* (light red plus) [37]; Cheung *et al.* (orange triangle) [28]; Cheung *et al.* (inverted orange triangle) [33]; Zhu *et al.* (dark blue square) [36]; Redondo-Yuste *et al.* (light blue diamond) [32]; and Mitmann *et al.* (light blue region) [29]. Since, the result given in Mitmann *et al.* [29] is for a range of values for the magnitude and phase of the QQNM ratio, we have therefore plotted this as a region in the contour plot.

Results.—We specialise to the scenario described above, with first-order pure QNM data consisting of a single regular and mirror mode, as in (13). The ensuing nonzero pieces of the second-order Weyl scalar are of the form (15)–(17). For concreteness, we display results for the QQNM mode with frequency $2s_{\ell m n}$, which corresponds to the expression in Eq. (15).

Typically, one is not directly interested in the value of $(\Psi_{4L}^{(2)})^{LM}$ at \mathcal{J}^+ , but in how it compares to the first-order perturbation. Since $\Psi_{4L}^{(2)} \sim (\Psi_4^{(1)})^2$, we might consider the following ratio:

$$(\mathcal{R}^{\Psi_4})^{LM} := \frac{(\Psi_{4L}^{(2)})^{LM}}{A_{\ell m n}^2}. \quad (18)$$

However, for comparison with the literature, it is more convenient to define the analogous ratio from the strain h , related to the Weyl scalar by $\Psi_4 \sim \dot{h}$. Employing the SpEC conventions (which notably use a re-scaled Kinnersley tetrad) [36], we arrive at the relation

$$(\mathcal{R}^{h_{\text{SpEC}}})^{LM} = -s_{\ell m n}^2 (\mathcal{R}^{\Psi_4})^{LM}. \quad (19)$$

Note that, apart from numerical factors, these ratios only depend on the ratio between mirror and regular mode amplitudes, $A_{\ell - m n}^*/A_{\ell m n}$. For example, $(\mathcal{R}^{\Psi_4})^{LM} = a^{LM}(0) + b^{LM}(0)A_{\ell - m n}^*/A_{\ell m n}$. Using Eqs. (7) and (8), we can alternatively express $(\mathcal{R}^{\Psi_4})^{LM}$ in terms of the ratio of odd to even amplitudes, $C_{\ell m n}^-/C_{\ell m n}^+$. In Kerr spacetime $(\mathcal{R}^{\Psi_4})^{LM}$ is also a function of the BH parameters and $C_{\ell m n}^-/C_{\ell m n}^+$. This can be derived by inputting Eq. (12) into the expression for the source, $\tilde{\mathcal{S}}$, available in Ref. [60]. This shows that the source consists of terms $\propto \bar{\Phi}^2$ and $\propto \Phi\bar{\Phi}$. Hence, using Eqs. (11), (13), and (5), similar relations as Eqs. (15) to (17) hold in Kerr (up to angular mode mixing) and $(\mathcal{R}^{\Psi_4})^{LM}$ is a function of $C_{\ell m n}^-/C_{\ell m n}^+$ and the BH parameters.

In Fig. 1, we show a contour plot of $(\mathcal{R}^{h_{\text{SpEC}}})^{LM}$ as a function of $C_{\ell m n}^-/C_{\ell m n}^+$ for the case $(\ell, m, n) = (2, 2, 0)$. We also include previous results from the literature in this plot. We relegate to the Supplemental Material how the data points were added to the figure. Notably, one should distinguish the results reported by Ma *et al.* [34] (dark red cross), which differ significantly from NR

results (in blue and orange), and from the BHPT result reported by Bucciotti *et al.* [37] (light red plus). In Ma *et al.*, the reported ratio (in Schwarzschild) has magnitude ≈ 0.137 and phase ≈ -0.083 . Their computation of this result assumed that $\Psi_4^{(1)}$ is composed of a single regular frequency, $s_{\ell m}$, with $A_{\ell - m} = 0$. Equivalently, they assume $C_{\ell m}^- = iC_{\ell m}^+$. We find that we exactly recover their result for $(\mathcal{R}^{h_{\text{SPEC}}})^{LM}$ in our framework, given their specific ratio $C_{\ell m}^-/C_{\ell m}^+$.

In contrast, the NR results we consider here (which typically consider mergers of spinning BHs that produce a BH remnant with small spin) give consistently larger magnitudes for the ratio, typically ranging from 0.15 to 0.20. Our figure shows, even neglecting systematic errors in the NR simulations, this discrepancy can be fully explained by the fact that odd-parity modes are typically subdominant in binary mergers, so that $|C_{\ell m}^-/C_{\ell m}^+|$ is significantly smaller than in the semi-analytical calculations [34]. This is a consequence of mild deviation from equatorial symmetry: for a perfectly up-down symmetric system, odd-parity modes identically vanish for even values of $\ell + m$ (meaning, in particular, for $\ell = m = 2$). In linear perturbation theory, this implies the odd-parity $\ell = m = 2$ modes identically vanish for nonspinning binary mergers.

Discussion.—Precision BH spectroscopy is expected to be a pillar of future GW astronomy, enabling stringent tests of GR and of whether the massive objects in galactic centers are described by the Kerr spacetime. This program is now widely expected to require calculations of QQNMs. In this Letter, we have shown how disagreements in recent QQNM calculations can be reconciled: both even- and odd-parity linear QNMs (or equivalently, regular and mirror modes) contribute to the same QQNM, and the discrepancies in the literature are due to differences in the relative excitations of the even and odd sectors. Most importantly, we have shown that in vacuum GR this is the unique way in which the QQNM amplitudes depend on the system that formed the BH (beyond the fact that the BH mass and spin also depend on the progenitor system). Our results therefore suggest that measurements of QQNMs can be used to extract how much the first-order even and

odd sectors have been excited, providing a unique route to determining, for example, the breaking of isospectrality in beyond-GR theories or due to environmental effects.

Given our results, an important task for future work will be to explore how the ratio $C_{\ell m}^-/C_{\ell m}^+$ depends on the details of the binary that formed the final BH. This would, in principle, make it simple to assess how the QQNM ratio depends on the BH's formation.

The results presented here were restricted to Schwarzschild, but our main conclusion and our computational framework generalise readily to Kerr. A companion paper will provide details of the framework and will be released with a complete code in Schwarzschild that can easily handle any number of first-order QNMs.

Acknowledgments.—We gratefully acknowledge helpful discussions with Sizheng Ma, Huan Yang, and Neev Khara. AS would like to thank Laura Sberna and Stephen Green for their helpful discussions. BL would like to thank Sebastian Völkel and Hector Okada da Silva for their helpful discussions. RPM thanks Jaime Redondo-Yuste for valuable discussions. PB and BB acknowledge the support of the Dutch Research Council (NWO) (project name: Resonating with the new gravitational-wave era, project number: OCENW.M.21.119). RPM acknowledges support from the Villum Investigator program supported by the VILLUM Foundation (grant no. VIL37766) and the DNRF Chair program (grant no. DNRF162) by the Danish National Research Foundation and the European Union's Horizon 2020 research and innovation programme under the Marie Skłodowska-Curie grant agreement No 101131233. AS acknowledges support from the STFC Consolidated Grant no. ST/V005596/1. AP acknowledges the support of a Royal Society University Research Fellowship and a UKRI Frontier Research Grant (as selected by the ERC) under the Horizon Europe Guarantee scheme [grant number EP/Y008251/1].

Note added—A recent paper appeared [37] while this paper was in preparation, which also emphasised the importance of the mirror modes in QQNM analysis. Their results are compatible with the results in this paper, but they make specific choices of even and odd parity ratios rather than characterizing the full dependence.

-
- [1] K. D. Kokkotas and B. G. Schmidt, Quasinormal modes of stars and black holes, *Living Rev. Rel.* **2**, 2 (1999), [arXiv:gr-qc/9909058](#).
 - [2] E. Berti, V. Cardoso, and A. O. Starinets, Quasinormal modes of black holes and black branes, *Class. Quant. Grav.* **26**, 163001 (2009), [arXiv:0905.2975 \[gr-qc\]](#).
 - [3] R. A. Konoplya and A. Zhidenko, Quasinormal modes of black holes: From astrophysics to string theory, *Rev. Mod. Phys.* **83**, 793 (2011), [arXiv:1102.4014 \[gr-qc\]](#).
 - [4] E. Barausse, V. Cardoso, and P. Pani, Can environmental effects spoil precision gravitational-wave astrophysics?, *Phys. Rev. D* **89**, 104059 (2014), [arXiv:1404.7149 \[gr-qc\]](#).
 - [5] O. Dreyer, B. J. Kelly, B. Krishnan, L. S. Finn, D. Garrison, and R. Lopez-Aleman, Black hole spectroscopy: Testing general relativity through gravitational wave observations, *Class. Quant. Grav.* **21**, 787 (2004), [arXiv:gr-qc/0309007 \[gr-qc\]](#).
 - [6] E. Berti, V. Cardoso, and C. M. Will, On gravitational-wave spectroscopy of massive black holes with the space interferometer LISA, *Phys. Rev. D* **73**, 064030 (2006), [arXiv:gr-qc/0512160](#).
 - [7] E. Berti, A. Sesana, E. Barausse, V. Cardoso, and K. Belczynski, Spectroscopy of Kerr black holes with Earth- and space-based interferometers, *Phys. Rev. Lett.* **117**, 101102 (2016), [arXiv:1605.09286 \[gr-qc\]](#).
 - [8] B. P. Abbott *et al.* (LIGO Scientific, Virgo), Observation

- of Gravitational Waves from a Binary Black Hole Merger, *Phys. Rev. Lett.* **116**, 061102 (2016), [arXiv:1602.03837 \[gr-qc\]](#).
- [9] R. Abbott *et al.* (LIGO Scientific, Virgo), Tests of general relativity with binary black holes from the second LIGO-Virgo gravitational-wave transient catalog, *Phys. Rev. D* **103**, 122002 (2021), [arXiv:2010.14529 \[gr-qc\]](#).
- [10] R. Abbott *et al.* (LIGO Scientific, VIRGO, KAGRA), Tests of General Relativity with GWTC-3, (2021), [arXiv:2112.06861 \[gr-qc\]](#).
- [11] M. Isi, M. Giesler, W. M. Farr, M. A. Scheel, and S. A. Teukolsky, Testing the no-hair theorem with GW150914, *Phys. Rev. Lett.* **123**, 111102 (2019), [arXiv:1905.00869 \[gr-qc\]](#).
- [12] C. D. Capano and A. H. Nitz, Binary black hole spectroscopy: a no-hair test of GW190814 and GW190412, *Phys. Rev. D* **102**, 124070 (2020), [arXiv:2008.02248 \[gr-qc\]](#).
- [13] C. D. Capano, M. Cabero, J. Westerweck, J. Abedi, S. Kastha, A. H. Nitz, Y.-F. Wang, A. B. Nielsen, and B. Krishnan, Multimode Quasinormal Spectrum from a Perturbed Black Hole, *Phys. Rev. Lett.* **131**, 221402 (2023), [arXiv:2105.05238 \[gr-qc\]](#).
- [14] R. Cotesta, G. Carullo, E. Berti, and V. Cardoso, Analysis of Ringdown Overtones in GW150914, *Phys. Rev. Lett.* **129**, 111102 (2022), [arXiv:2201.00822 \[gr-qc\]](#).
- [15] C. D. Capano, J. Abedi, S. Kastha, A. H. Nitz, J. Westerweck, Y.-F. Wang, M. Cabero, A. B. Nielsen, and B. Krishnan, Statistical validation of the detection of a sub-dominant quasi-normal mode in GW190521, (2022), [arXiv:2209.00640 \[gr-qc\]](#).
- [16] X. J. Forteza, S. Bhagwat, S. Kumar, and P. Pani, Novel Ringdown Amplitude-Phase Consistency Test, *Phys. Rev. Lett.* **130**, 021001 (2023), [arXiv:2205.14910 \[gr-qc\]](#).
- [17] E. Finch and C. J. Moore, Searching for a ringdown overtone in GW150914, *Phys. Rev. D* **106**, 043005 (2022), [arXiv:2205.07809 \[gr-qc\]](#).
- [18] J. Abedi, C. D. Capano, S. Kastha, A. H. Nitz, Y.-F. Wang, J. Westerweck, A. B. Nielsen, and B. Krishnan, Spectroscopy for asymmetric binary black hole mergers, *Phys. Rev. D* **108**, 104009 (2023), [arXiv:2309.03121 \[gr-qc\]](#).
- [19] G. Carullo, R. Cotesta, E. Berti, and V. Cardoso, Reply to Comment on "Analysis of Ringdown Overtones in GW150914", *Phys. Rev. Lett.* **131**, 169002 (2023), [arXiv:2310.20625 \[gr-qc\]](#).
- [20] V. Baibhav, M. H.-Y. Cheung, E. Berti, V. Cardoso, G. Carullo, R. Cotesta, W. Del Pozzo, and F. Duque, Agnostic black hole spectroscopy: Quasinormal mode content of numerical relativity waveforms and limits of validity of linear perturbation theory, *Phys. Rev. D* **108**, 104020 (2023), [arXiv:2302.03050 \[gr-qc\]](#).
- [21] P. J. Nee, S. H. Völkel, and H. P. Pfeiffer, Role of black hole quasinormal mode overtones for ringdown analysis, *Phys. Rev. D* **108**, 044032 (2023), [arXiv:2302.06634 \[gr-qc\]](#).
- [22] H. Zhu, J. L. Ripley, A. Cárdenas-Avenidaño, and F. Pretorius, Challenges in quasinormal mode extraction: Perspectives from numerical solutions to the Teukolsky equation, *Phys. Rev. D* **109**, 044010 (2024), [arXiv:2309.13204 \[gr-qc\]](#).
- [23] H. Siegel, M. Isi, and W. M. Farr, Ringdown of GW190521: Hints of multiple quasinormal modes with a precessional interpretation, *Phys. Rev. D* **108**, 064008 (2023), [arXiv:2307.11975 \[gr-qc\]](#).
- [24] V. Gennari, G. Carullo, and W. Del Pozzo, Searching for ringdown higher modes with a numerical relativity-informed post-merger model, *Eur. Phys. J. C* **84**, 233 (2024), [arXiv:2312.12515 \[gr-qc\]](#).
- [25] M. Maggiore *et al.*, Science Case for the Einstein Telescope, *JCAP* **03**, 050, [arXiv:1912.02622 \[astro-ph.CO\]](#).
- [26] M. Cabero, J. Westerweck, C. D. Capano, S. Kumar, A. B. Nielsen, and B. Krishnan, Black hole spectroscopy in the next decade, *Phys. Rev. D* **101**, 064044 (2020), [arXiv:1911.01361 \[gr-qc\]](#).
- [27] A. Toubiana, L. Pompili, A. Buonanno, J. R. Gair, and M. L. Katz, Measuring source properties and quasinormal-mode frequencies of heavy massive black-hole binaries with LISA, (2023), [arXiv:2307.15086 \[gr-qc\]](#).
- [28] M. H.-Y. Cheung *et al.*, Nonlinear Effects in Black Hole Ringdown, *Phys. Rev. Lett.* **130**, 081401 (2023), [arXiv:2208.07374 \[gr-qc\]](#).
- [29] K. Mitman *et al.*, Nonlinearities in Black Hole Ringdowns, *Phys. Rev. Lett.* **130**, 081402 (2023), [arXiv:2208.07380 \[gr-qc\]](#).
- [30] Y. Zlochower, R. Gomez, S. Husa, L. Lehner, and J. Winicour, Mode coupling in the nonlinear response of black holes, *Phys. Rev. D* **68**, 084014 (2003), [arXiv:gr-qc/0306098](#).
- [31] L. Sberna, P. Bosch, W. E. East, S. R. Green, and L. Lehner, Nonlinear effects in the black hole ringdown: Absorption-induced mode excitation, *Phys. Rev. D* **105**, 064046 (2022), [arXiv:2112.11168 \[gr-qc\]](#).
- [32] J. Redondo-Yuste, G. Carullo, J. L. Ripley, E. Berti, and V. Cardoso, Spin dependence of black hole ringdown nonlinearities, (2023), [arXiv:2308.14796 \[gr-qc\]](#).
- [33] M. H.-Y. Cheung, E. Berti, V. Baibhav, and R. Cotesta, Extracting linear and nonlinear quasinormal modes from black hole merger simulations, (2023), [arXiv:2310.04489 \[gr-qc\]](#).
- [34] S. Ma and H. Yang, The excitation of quadratic quasinormal modes for kerr black holes (2024), [arXiv:2401.15516 \[gr-qc\]](#).
- [35] S. Yi, A. Kuntz, E. Barausse, E. Berti, M. H.-Y. Cheung, K. Kritos, and A. Maselli, Nonlinear quasinormal mode detectability with next-generation gravitational wave detectors, (2024), [arXiv:2403.09767 \[gr-qc\]](#).
- [36] H. Zhu *et al.*, Nonlinear effects in black hole ringdown from scattering experiments: Spin and initial data dependence of quadratic mode coupling, *Phys. Rev. D* **109**, 104050 (2024), [arXiv:2401.00805 \[gr-qc\]](#).
- [37] B. Bucciotti, L. Juliano, A. Kuntz, and E. Trincerini, Quadratic Quasi-Normal Modes of a Schwarzschild Black Hole, (2024), [arXiv:2405.06012 \[gr-qc\]](#).
- [38] R. Panosso Macedo and M. Ansorg, Axisymmetric fully spectral code for hyperbolic equations, *J. Comput. Phys.* **276**, 357 (2014), [arXiv:1402.7343 \[physics.comp-ph\]](#).
- [39] M. Ansorg and R. Panosso Macedo, Spectral decomposition of black-hole perturbations on hyperboloidal slices, *Phys. Rev. D* **93**, 124016 (2016), [arXiv:1604.02261 \[gr-qc\]](#).
- [40] M. Ammon, S. Grieninger, A. Jimenez-Alba, R. P. Macedo, and L. Melgar, Holographic quenches and anomalous transport, *JHEP* **09**, 131, [arXiv:1607.06817 \[hep-th\]](#).
- [41] R. Panosso Macedo, J. L. Jaramillo, and M. Ansorg, Hyperboloidal slicing approach to quasi-normal mode

- expansions: the Reissner-Nordström case, *Phys. Rev. D* **98**, 124005 (2018), [arXiv:1809.02837 \[gr-qc\]](#).
- [42] R. Panosso Macedo, Hyperboloidal framework for the Kerr spacetime, *Class. Quant. Grav.* **37**, 065019 (2020), [arXiv:1910.13452 \[gr-qc\]](#).
- [43] J. L. Jaramillo, R. Panosso Macedo, and L. Al Sheikh, Pseudospectrum and Black Hole Quasinormal Mode Instability, *Phys. Rev. X* **11**, 031003 (2021), [arXiv:2004.06434 \[gr-qc\]](#).
- [44] R. Panosso Macedo, Hyperboloidal approach for static spherically symmetric spacetimes: a didactical introduction and applications in black-hole physics, *Phil. Trans. Roy. Soc. Lond. A* **382**, 20230046 (2024), [arXiv:2307.15735 \[gr-qc\]](#).
- [45] R. Panosso Macedo, B. Leather, N. Warburton, B. Wardell, and A. Zenginoğlu, Hyperboloidal method for frequency-domain self-force calculations, *Phys. Rev. D* **105**, 104033 (2022), [arXiv:2202.01794 \[gr-qc\]](#).
- [46] A. Spiers, A. Pound, and B. Wardell, Second-order perturbations of the Schwarzschild spacetime: practical, covariant and gauge-invariant formalisms, [arXiv:2306.17847 \[gr-qc\]](#) (2023).
- [47] A. Spiers, A. Pound, and J. Moxon, Second-order Teukolsky formalism in Kerr spacetime: Formulation and nonlinear source, *Phys. Rev. D* **108**, 064002 (2023), [arXiv:2305.19332 \[gr-qc\]](#).
- [48] A. Pound and B. Wardell, Black hole perturbation theory and gravitational self-force [10.1007/978-981-15-4702-7_38-1](#) (2021), [arXiv:2101.04592 \[gr-qc\]](#).
- [49] S. A. Teukolsky, Rotating black holes: Separable wave equations for gravitational and electromagnetic perturbations, *Physical Review Letters* **29**, 1114 (1972).
- [50] S. A. Teukolsky, Perturbations of a rotating black hole. i. fundamental equations for gravitational, electromagnetic, and neutrino-field perturbations, *Astrophysical Journal*, Vol. 185, pp. 635-648 (1973) **185**, 635 (1973).
- [51] E. W. Leaver, Spectral decomposition of the perturbation response of the Schwarzschild geometry, *Phys. Rev. D* **34**, 384 (1986).
- [52] A. Zenginoglu, A Geometric framework for black hole perturbations, *Phys. Rev. D* **83**, 127502 (2011), [arXiv:1102.2451 \[gr-qc\]](#).
- [53] H.-P. Nollert, About the significance of quasinormal modes of black holes, *Phys. Rev. D* **53**, 4397 (1996), [arXiv:gr-qc/9602032](#).
- [54] A. Dhani, Importance of mirror modes in binary black hole ringdown waveform, *Physical Review D* **103**, 104048 (2021).
- [55] T. Mädler and J. Winicour, Bondi-Sachs Formalism, *Scholarpedia* **11**, 33528 (2016), [arXiv:1609.01731 \[gr-qc\]](#).
- [56] K. Martel and E. Poisson, Gravitational perturbations of the Schwarzschild spacetime: A Practical covariant and gauge-invariant formalism, *Phys. Rev. D* **71**, 104003 (2005), [arXiv:gr-qc/0502028](#).
- [57] M. Campanelli and C. O. Lousto, Second order gauge invariant gravitational perturbations of a kerr black hole, *Physical Review D* **59**, 124022 (1999).
- [58] S. R. Green, S. Hollands, and P. Zimmerman, Teukolsky formalism for nonlinear Kerr perturbations, *Classical and Quantum Gravity* **37**, 075001 (2020).
- [59] A. Spiers, B. Wardell, A. Pound, S. D. Upton, and N. Warburton, [PerturbationEquations](#) (2024).
- [60] A. Spiers, NP and GHP Formalisms for second-order Teukolsky equations,

<https://github.com/DrAndrewSpiers/NP-and-GHP-Formalisms-for-2nd-order-Teukolsky> (2023).

SUPPLEMENTAL MATERIAL

(ℓ, m, n)	at J^+ ($\sigma = 0$)	
(2, 2, 0)	s_{220}	$-0.08896 - 0.37367i$
	a^{44}	$0.8614 + 0.347958i$
	b^{44}	$0.0969646 + 0.0564975i$
	a^{40}	3.76953×10^{-5}
	b^{40}	$(0.136826 - 8.7888i) \times 10^{-5}$
(3, 3, 0)	s_{330}	$0.0927 + 0.5994i$
	a^{66}	$0.55259 + 0.0645167i$
	b^{66}	$-0.0680453 - 0.0370004i$
	a^{60}	4.27944×10^{-7}
	b^{60}	$10^{-6}(-7.59687 + 8.14475i)$
(4, 4, 0)	s_{440}	$0.09416 + 0.8092i$
	a^{88}	$0.318602 - 0.00475926i$
	b^{88}	$0.0410101 + 0.0194345i$
	a^{80}	1.2004×10^{-8}
	b^{80}	$(1.13628 - 0.744193i) \times 10^{-6}$

TABLE I: Values of $s_{\ell mn}$ and of the coefficients at J^+ appearing in Eqs (15)-(17), for a selection of mode numbers (ℓ, m, n) .

References	$(\mathcal{R}^{h_{\text{SpEC}}})^{44}$
Ma <i>et al.</i> [34]	$0.137e^{-0.083i}$
Bucciotti <i>et al.</i> [37]	$0.154e^{-0.068i}$
Cheung (1) <i>et al.</i> [28]	$0.1637e^{0.177i}$
Cheung (2) <i>et al.</i> [33]	$0.170e^{0.077i}$
Zhu <i>et al.</i> [36]	(by eye) $0.17e^{-0.083i}$
Mitmann <i>et al.</i> [29]	$(0.15 : 0.20)e^{(-0.4:0.4)i}$
Redondo-Yuste <i>et al.</i> [32]	$0.164e^{-0.065i}$

TABLE II: The reported values for the magnitude and phase of the QQNM ratio $(\mathcal{R}^{h_{\text{SpEC}}})^{44}$.

In Table I, we give the values for the frequencies $s_{\ell mn}$ and the coefficients appearing in Eqs (15)-(17), evaluated at J^+ ($\sigma = 0$), for different ℓm modes. For completeness, we give in Table II the QQNM ratios as reported in the literature that are used to generate the data points in Fig. 1. These data points were computed in the following manner:

To include the data from Table II in Fig. 1, we must extract the ratio $C_{\ell mn}^-/C_{\ell mn}^+$ from the data. We do this starting from the values of the magnitude and phase of the QQNM ratio, $(\mathcal{R}^{h_{\text{SpEC}}})^{LM}$ (as given in the cited references). Using relations (19), (18), and (15), together with Eqs. (7) and (8), we then calculate the (unique) complex ratio $C_{\ell mn}^-/C_{\ell mn}^+$. We can then plot the corresponding point in the complex plane, as shown in Fig. 1.